BEAM FOIL ATOMIC SPECTROSCOPY

L. J. CURTIS
Department of Physics and Astronomy, University of Toledo,
Toledo Ohio USA

Introduction

The research technique of Beam Foil Spectroscopy (BFS) provides a fitting subject for presentation at a conference on accelerators, since its broad applicability can be achieved only through access to a wide range of accelerator types and energy ranges. The method is now a mature field of study (having been pursued for over 30 years), and has provided much new data, elucidated fundamental atomic processes, and furthered applications in many fields. New technical capabilities have now broadened the field to permit new types of measurements of unprecedented accuracy and scope. The international nature of this work is also being extended, with active groups in, e.g. China, India, Japan, and South Africa. In this talk, I would like to review some of the successful applications of the method, and indicate other areas that hold promise for future measurements.

Some of the unique characteristics of this light source are described in Slide 1. As is often the case, strengths often also impose limitations, but many features that were earlier considered as limitations have now been reduced or eliminated. Given a suitable accelerator and ion source, virtually any ion of any atom can be studied in a time-resolved manner. Since the time-resolution is achieved by time-of-flight methods, this imposes limitations on the minimum and maximum time windows. The solid foil provides a region of very high density that causes heavy excitation of all levels, including extensive core excitations. This involves nonselective excitation, so that decay curves are sums of many exponentials because of cascade repopulation. The density of the beam is very low (much rarer than the residual gas even at very high vacuum) so there are no collisions, radiation damping, or stray fields. This also leads to low light levels, which require fast optics with significant acceptance apertures, hence the high velocity of the beam leads to Doppler broadening of the lines. Because the beam suddenly emerges

from the dense foil into the evacuated flight path, the excitation can be coherent, exhibiting interference and quantum beats. The preferred direction and the possibility of tilting the foil can produce excitation anisotropies. In recent years, methods have been developed that now eliminate or minimize many of the earlier shortcomings.

Slide 1

Beam Foil Spectroscopy

Universal:	**Any ion of any atom (Limited time window)**
High density excitation:	**Large fraction excited; Multiple excitation (Non selective; cascades and blends**
Low density decay:	**No collisions; no trapping; no Stark quenching metastables decay radiative (low light levels)**
Coherent and anisotropic:	**Transition form high density to vacuum sudden; phases entangled; quantum beats, polarization**
Resolution:	**50 mÅ/refocussing; 10 ps/high optical resolution**

Nominal lifetime resolution: 2-8%

The attributes of the BFS light source are clearly manifested by its visual appearance. Slide 2 shows a 700 keV (v=4.4 mm/ns) Li beam exiting a foil. The blue light near the foil is from a H-like Li^{2+} transition with lifetime 3 ns and the green light is from a He-like Li^{+} transition of lifetime 44 ns. Lifetime measurements are usually obtained by stepwise translating the foil upstream and downstream while the optics views a fixed point along the beam.

Slide 2

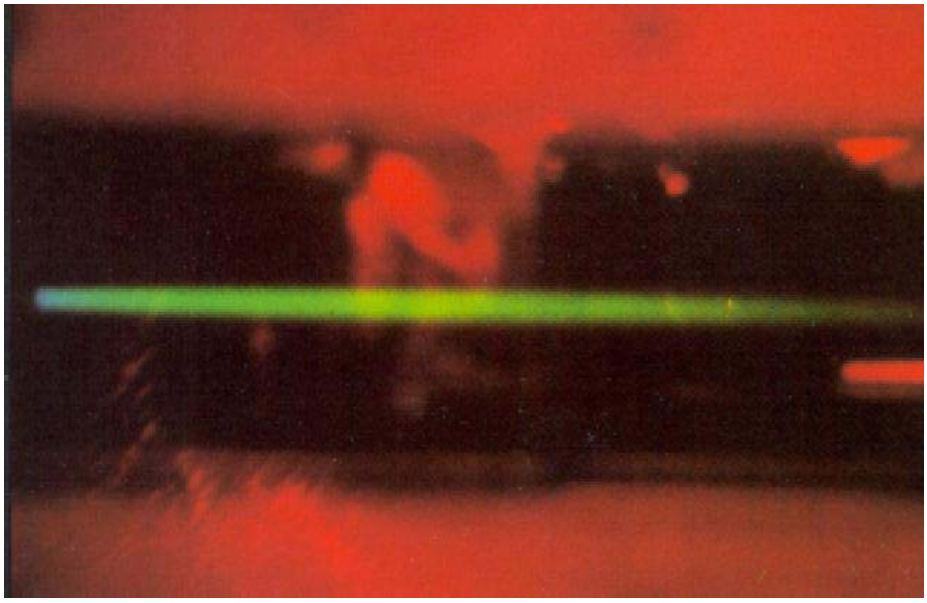

Technical Developments and Applications

A means for reducing the Doppler broadening is shown in Slide 3. The upper inset represents a spectrometer with a concave grating viewing a stationary light source, producing a focus at the exit slit. The lower inset illustrates how a moving light source has an angular correlation in the Doppler shift, leading to a differing angle of interference over the surface of the grating. Thus, by "refocusing the spectrometer to a moving light source" (moving either the grating or the exit slit in a wavelength- and velocity-dependent way) the Doppler broadened profile is converted into a narrow "purple shifted" line.

A solution to the problem of cascade repopulation is illustrated in Slide 4. This is known as the method of Arbitrarily Normalized Decay Curves (ANDC). The instantaneous rate of population change of given level is governed by the intensity of cascades into and decays out of that level.

Slide 3

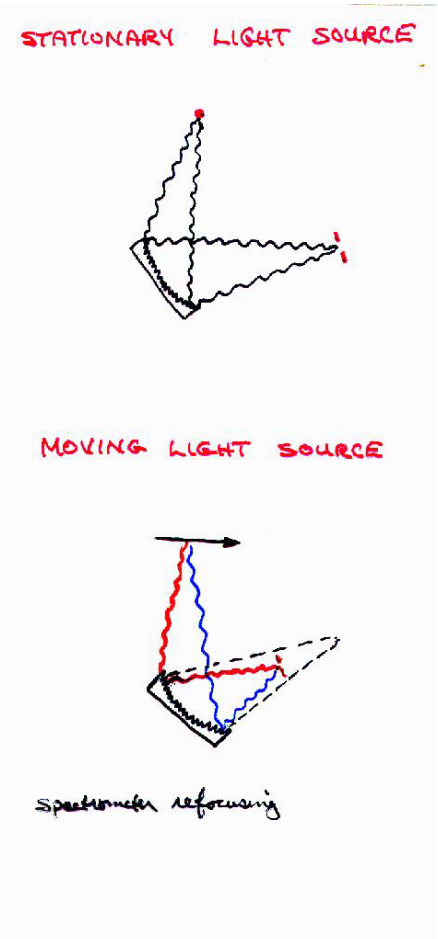

To within factors of the transition probabilities and detection efficiencies, the time dependence of these populations is specified by the variation of the detected intensities along the time-resolved decay curves. Thus, rather than expanding a single decay curve measurement on a set of mathematical exponentials, it is possible to expand the decay curve of the primary level on the measured decay curves of the cascades that repopulate it. In this formulation the lifetime and the detection efficiencies can be accurately extracted as linear fitting parameters, with

consistency checks to assure that all significant cascades have been included. A schematic representation of such a determination of the lifetime of the 6p level in Tl^{2+} is shown in Slide 5. Decay curves of the 6p, 6d and 7s were measured by beam-foil methods and jointly ANDC analyzed. This method has been used to obtain many lifetimes of high reliability and precision.

Slide 4

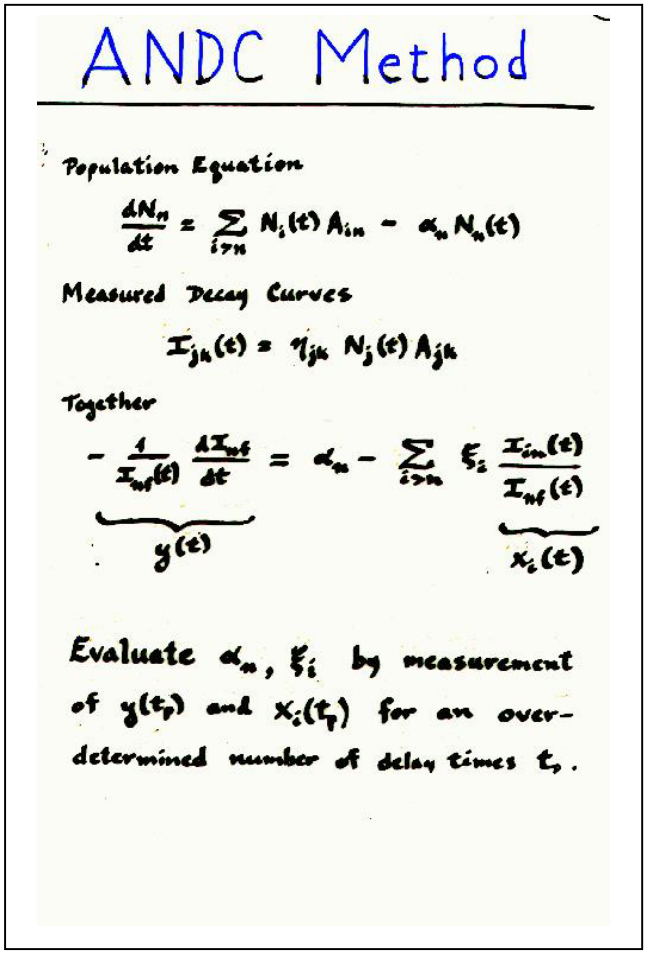

Slide 5

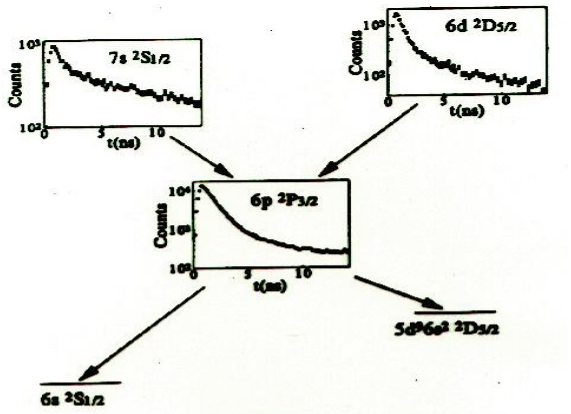

FIG. 2. Schematic representation of the ANDC method as applied to the decay curves of the $6p$ level and its cascades from $6d$ and $7s$. Using Eq. (10), each value of t_i provides a separate relationship by which the primary lifetime and the relative normalizations of the cascade decay can be determined.

$$\tau_{6p}\frac{dI_{6p}}{dt}(t_i)=\xi_{6d}I_{6d}(t_i)+\xi_{7p}I_{7p}(t_i)-I_{6p}(t_i). \quad (10)$$

One of the most serious limitations of the method has been the low intensity of the emitted light. This was exacerbated by the fact that the time-of-flight method involves single channel detection, in which the time-since-excitation is measured in a multiscaling mode. The limitations of this method have been greatly reduced by the development of position sensitive detectors (PSD). While detection is still single channel in the time domain, it is now possible to achieve multiplexed detection in wavelength. By simultaneously measuring a broad range of wavelengths at each time since excitation, many advantages are achieved. This is illustrated in Slide 6. By virtue of simultaneous measurement, many possible systematic uncertainties are eliminated in differences between the decay curves. It is also possible to examine the exponential content across a line profile to check for line blending. For systems in which the wavelengths of the primary and cascade transitions lie within the multiplexed wavelength range, it is possible to perform ANDC analysis in real time.

Slide 6

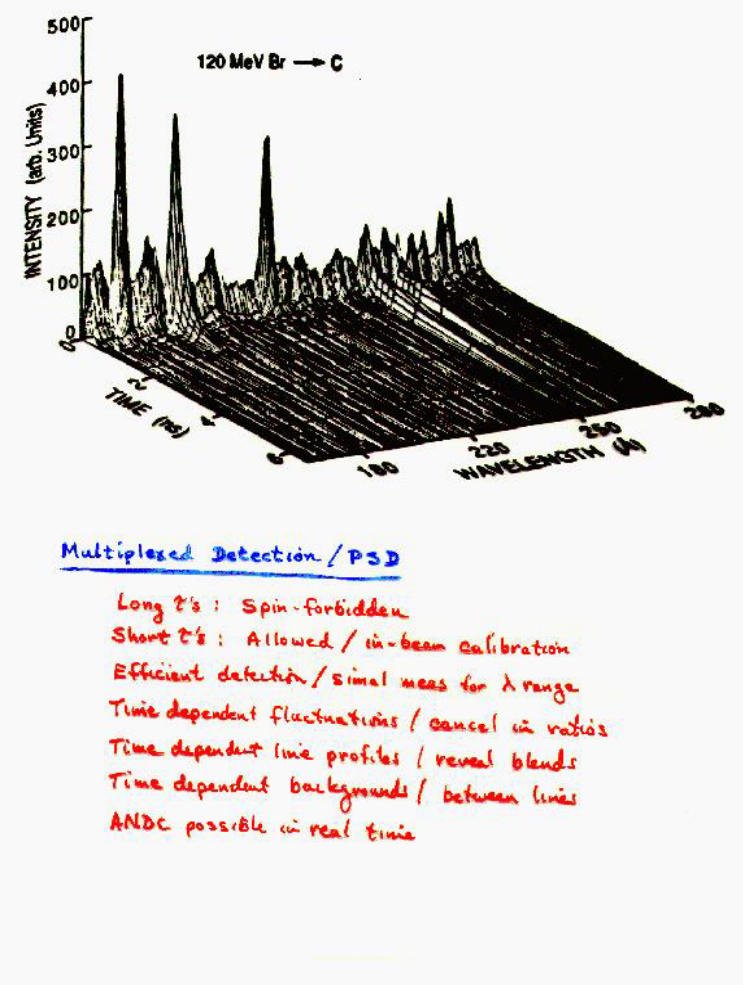

Another advantage is shown in Slide 7. In this system the J=1 fine structure level of the Be-like 2s3p triplet term possesses an additional E1 decay channel to ground that is forbidden to the J=0 and 2 levels by angular momentum conservation. The transition probability for this channel can be specified by differential decay curve measurements.

Prior to the availability of PSD devices, these decay curves were measured separately and subtracted channel-by-channel. If the emitted radiation from all three of these transitions is detected simultaneously at each distance downstream, many systematic uncertainties will cancel in differential measurements, and the precision will be greatly enhanced over previous determinations. In this example an extra channel to the ground state is determined by differential lifetime measurements. In a similar manner, multiply excited ions sometimes possess a *J*-dependent autoionization channel that can be determined by using these same differential lifetime measurement methods.

Slide 7

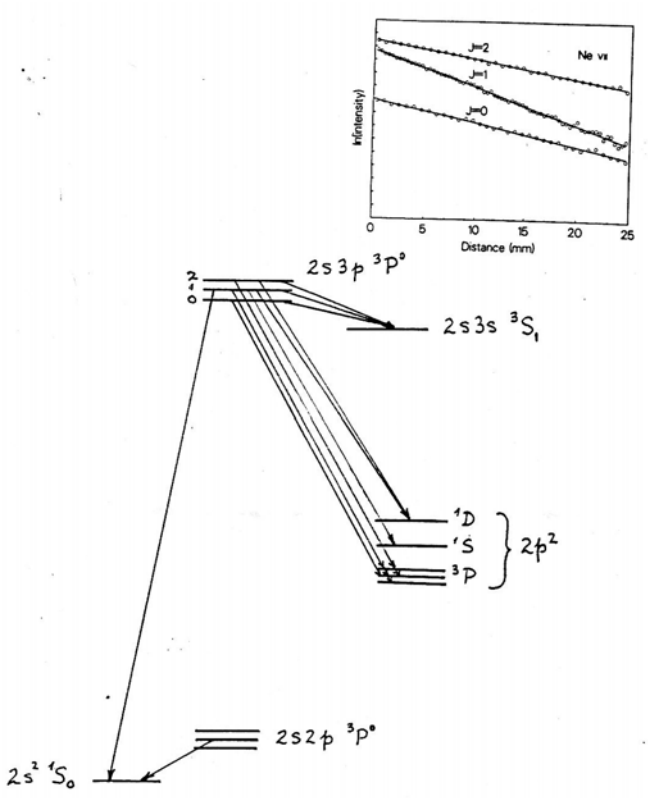

Slide 8 shows a measurement of the quantum beats that arise from coherent excitation of fine structure levels in He I. These relative frequency measurements were made with a common time base by using two different spectrometers so as to obtain a precise relative normalization. Similar measurements can now be made through PSD detection, and could provide precise accurate relative values for fine and hyperfine structure splittings.

Slide 8

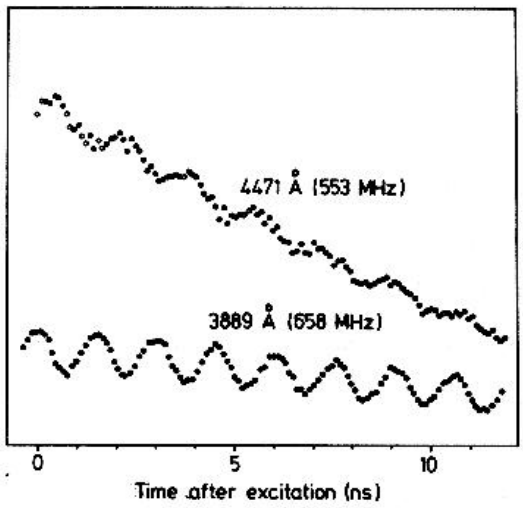

.

Isoelectronic Measurements

One particularly valuable application of BFS has been the study of lifetimes along isoelectronic sequences. By utilizing a variety of accelerators to trace a sequence of ions with a fixed number of electrons as a function of nuclear charge *Z*, it possible to examine and separate processes that scale differently with *Z*. For highly charged ions, properties are often different from those observed for neutral and few times ionized systems (e.g., magnetic fine structure can exceed electrostatic gross structure, forbidden transitions can exceed allowed transitions, etc.).

This power of these isoelectronic studies is illustrated by the semiempirical methods developed in Lund by Bengt Edlén. Slide 9 shows a plot of the scaled line strength factors for the lowest resonance transitions of the alkali-metallike isoelectronic sequences. All line strength factors (and their uncertainties) for charged ions on this plot were deduced from beam-foil lifetime measurements, many using the ANDC method. Professor Edlén showed that these quantities exhibit a nearly linear behavior when plotted vs a suitably chosen reciprocal screened charge. Moreover, it has been subsequently observed that this linearity appears to extrapolate to the hydrogenic limit at infinite *Z*. While this extreme limit is clearly a nonphysical asymptote, tests can be made to determine whether or not this linear behavior persists through all of the stable isotopes.

Slide 9

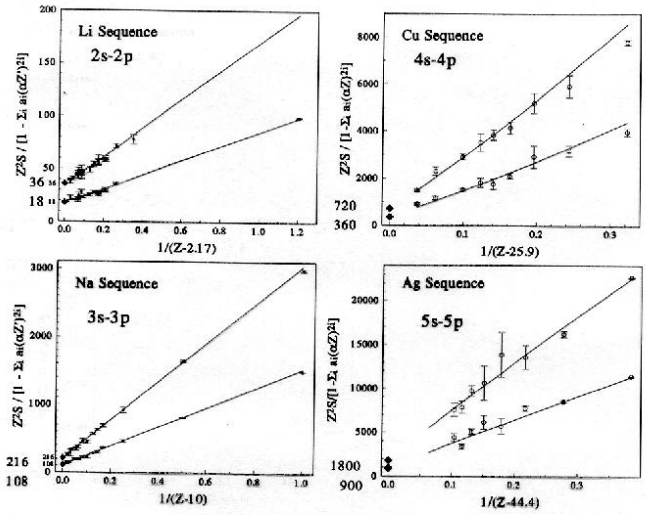

$$S_H = \frac{3}{4} n^2 (n^2 - 1)(2J_u + 1)$$

$$S = \left[\frac{\lambda(\text{Å})}{1265.38}\right]^2 \frac{1}{\tau(\text{ns})}$$

Slide 10

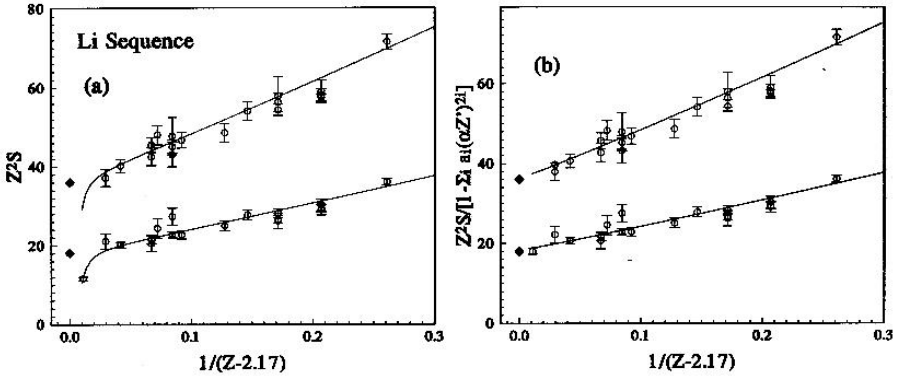

Results for Li-like uranium are shown in the left inset of Slide 10, and indicate a dip in value below the linear trend. (Again, all values shown here were deduced from beam-foil lifetime measurements.) Alternative models for the origin for this dip can be considered. One model is that a many-electron redistribution of the electrons in the complex core is occurring. A second model is that relativistic corrections to the single electron definition of the line strength factor must be included. (A third model is that both effects are significant.) It is possible to examine these two models semiempirically. Higher order calculations were made using the Dirac equation rather than the Schrödinger equation, and used to correct the abscissae of the measured data points. As shown in the right inset of Slide 10, this second model successfully restored the linearity. Subsequent theoretical calculations have confirmed this result. Because of this linearity, it is now possible to interpolate, extrapolate, and smooth data throughout entire isoelectronic sequences. This can be done on the basis of only a few accurate measurements, which serve to specify the screening parameter on the abscissa.

While these measurements now accurately specify all of the lifetimes of the lowest resonance transitions in alkali-metallike systems, other transitions in these systems still pose challenges for future measurements. Transition rates among the excited states in alkali-metallike systems are difficult to specify either theoretically or experimentally. In in Slide 11, a plot of the transition probabilities as a function of the effective quantum numbers of the upper and lower states

Slide 11

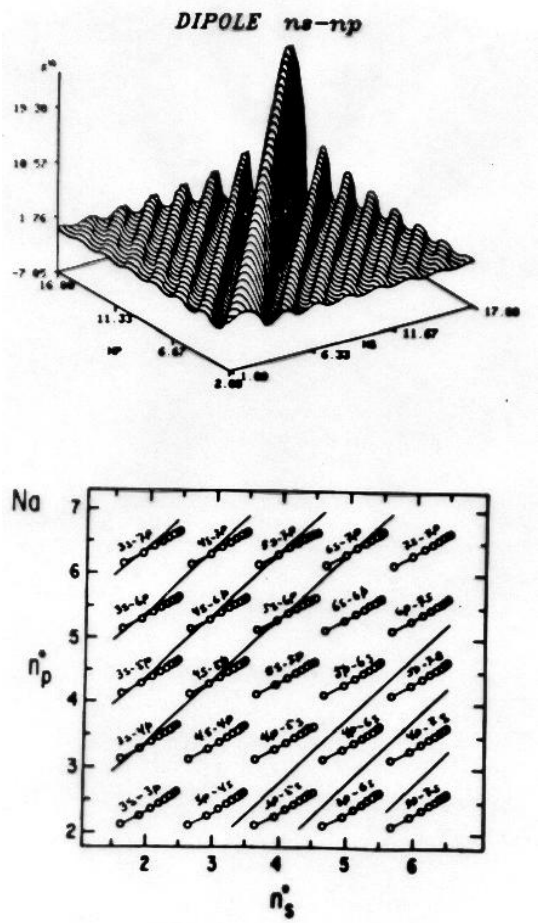

is shown, with values for the physical ions indicated by connected points. This exposition shows that theory is hindered by the many cancellations that occur in the transition integrals. Experimental measurements of line strength factors between excited levels are almost entirely lacking. These levels undergo branched decay, and lifetimes cannot be reduced to line strength factors without accompanying branching fraction data. Because of difficulties with relative in-beam intensity calibrations, branching fraction data in multiply charged ions

is virtually non-existent. However, new methods offer promise in this area, which will be discussed later in this paper.

Slide 12

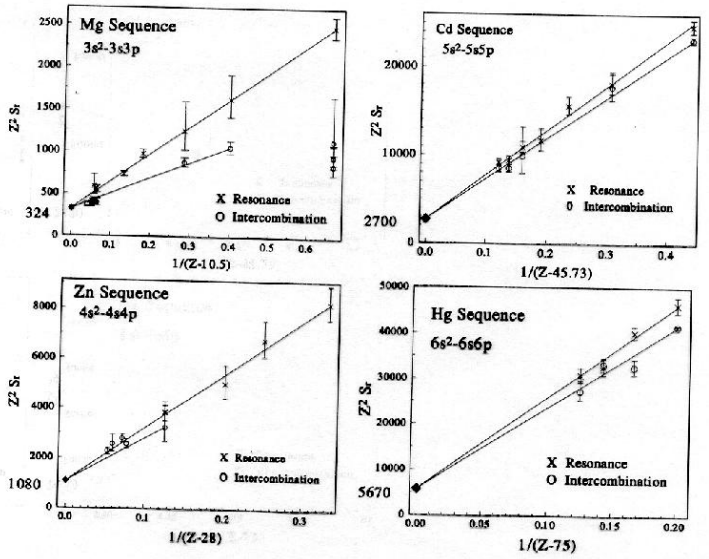

$$S_r(Res) = \frac{S(Res)}{\cos^2\vartheta} \qquad S_r(Int) = \frac{S(Int)}{\sin^2\vartheta}$$

ϑ determined from energy level data

These semiempirical methods can also be applied to two valence electron atoms, as shown in Slide 12. As for the alkali-metallike sequences, line strength factors for all multiply charged ions were deduced from beam-foil lifetime measurements, often using the ANDC method. Because of the singlet-triplet nature of these levels, the resonance and intercombination transitions to ground can be related to each other through intermediate coupling (IC) amplitudes describing the deviation of their angular momentum states from pure *LS* coupling. The IC amplitudes can be specified as mixing angles deduced from spectroscopic energy level data. Notice that, like the alkali-metallike case, these scaled line strength plots also exhibit a linearity that converges to the hydrogenic value at infinite *Z*. Moreover, as shown in

Slide 13, the singlet-triplet mixing angles can also be presented in a linearized plot that converges to the *jj* coupling limit at infinite *Z*.

Slide 13

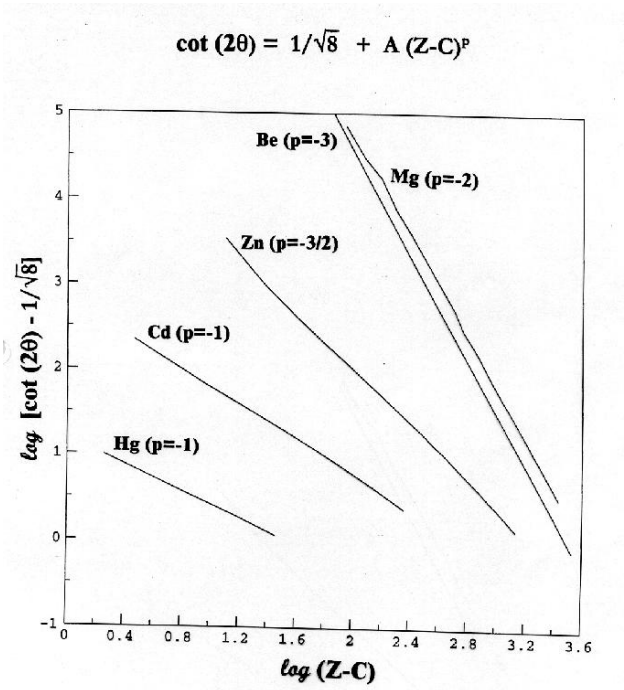

This formulation permits another type of test of relativistic corrections. In the nonrelativistic limit, the Schrödinger equation and *LS* coupling should be expected to hold, and govern the IC amplitudes. However, for very complex atoms, the use of the Dirac equation and *jj* coupling becomes necessary. In that limit, the spin dependence occurs not only in the angular momentum portion of the wave function, but also in the radial portion of the wave function. This generalization of the mixing angle formulation is shown in Slide 14. Perhaps not surprisingly, the reformulation relative to the *jj* limit yields a mixing angle that is very similar to that of the nonrelativistic case, but with a phase shift dictated by the difference between the radial matrix elements.

MCDF calculations for these quantities are shown in Slide 15, which indicate that these effects are negligible for all but the Hg isoelectronic sequence. The correction is most significant for the lower ions of the sequence, where the angular portion of the mixing is smallest. A plot of the mixing angle linearization, with and without this correction, is shown in Slide 16. The effect on the exposition of the line strength factors is shown in Slide 17. The application of this correction moved the Hg I and Tl II points onto the linear trend. Note that for this sequence only four stable ions exist, but the trend permits accurate predictions for the radioactive members of the sequence.

Slide 18 shows a similar analysis for the Ne isoelectronic sequence. Here the fact that the transitions have Δn=1 rather than Δn =0 results in much shorter lifetimes (because of the wavelength-cubed dependence). For highly charged ions these lifetimes are too short to be measured by time-of-flight and too long to be measured by line widths, but they have important applications in, eg, x-ray laser technology. Thus the accurate extrapolation of the measurements accessible to BFS measurements are valuable.

Slide 14

Dirac Formulation

For ns^2-$nsnp$ there are two radial wavefunctions $R_{2j,2j'}$

$$S(Res) \propto [R_{11}\cos(\theta_{jj} - \theta) - R_{31}\sin(\theta_{jj} - \theta)]^2$$

$$S(Int) \propto [R_{11}\sin(\theta_{jj} - \theta) + R_{31}\cos(\theta_{jj} - \theta)]^2$$

and the jj coupling limit

$$\tan\theta_{jj} = \sqrt{\tfrac{1}{2}}$$

reduces by trigonometric identities to

$$S_r(Res) \equiv \frac{S(Res)}{\cos^2(\theta - \xi)}$$

$$S_r(Int) \equiv \frac{S(Int)}{\sin^2(\theta - \xi)}$$

where

$$\tan\xi \equiv \sqrt{2}\frac{R_{31} - R_{11}}{2R_{31} + R_{11}}.$$

Slide 15

TABLE II: Ratios of radial matrix elements. Here $\Delta \equiv (R_{13}/R_{11} - 1)$ x 1000.

Charge	Ion	Δ	Ion	Δ	Ion	Δ	Ion	Δ	Ion	Δ
I	Be	0.037	Mg	-	Zn	-1.99	Cd	-6.74	Hg	-40.2
II	B	0.113	Al	0.18	Ga	+0.16	In	-1.30	Tl	-18.2
III	C	0.212	Si	0.41	Ge	1.00	Sn	+0.35	Pb	-12.5
IV	N	0.342	P	0.61	As	1.54	Sb	1.24	Bi	-10.3
V	O	0.503	S	0.82	Se	1.97	Te	1.78	Po	-9.20
VI	F	0.682	Cl	1.04	Br	2.37	I	2.26	At	-8.64
VII	Ne	0.888	Ar	1.29	Kr	2.75	Xe	2.66	Rn	-8.27

Slide 16

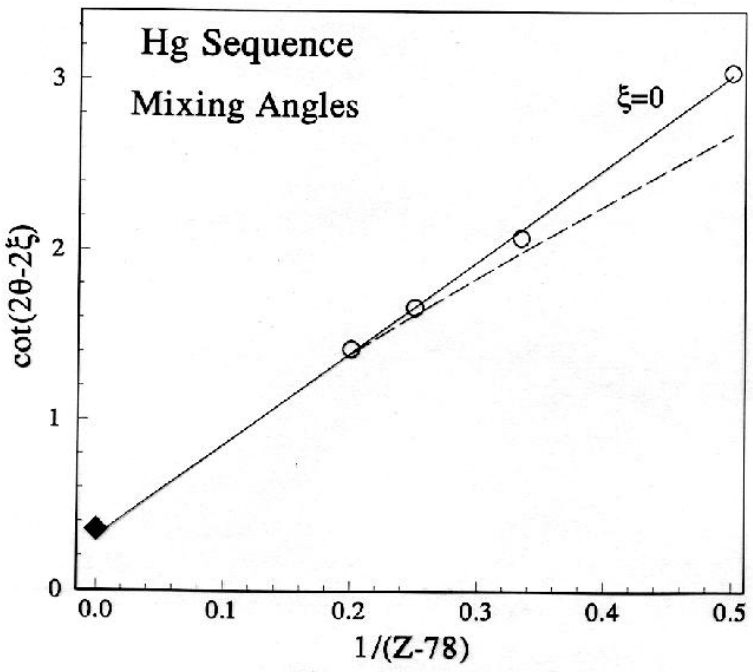

Slide 17

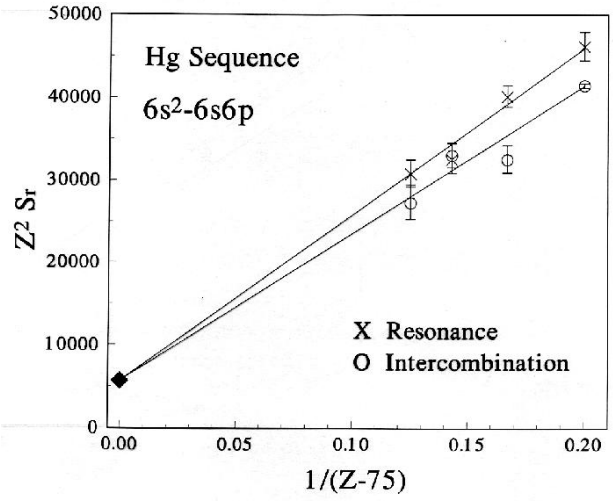

Slide 18

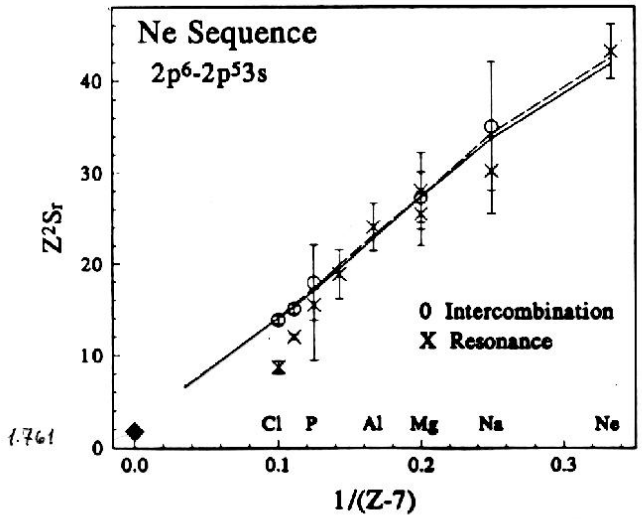

Calibration Standards

Isoelectronic measurements and semiempirical parametrizations can also be employed to obtain calibration standards. An example is shown in Slide 19 for the Pb isoelectronic sequence. The ground term can be specified by two mixing angles, and the excited term can be specified in terms of a third mixing angle. If these are nearly pure configurations (with little CI) then the relative transition rates should be specified by these three mixing angles. This has been applied to transitions in neutral Si, Ge and Sn, for which precision measurements of the branching fractions exist. As shown in Slide 20, the semiempirical calculations show striking agreement with the measured branching fractions. These results (together with the high accuracy to which the overdetermined mixing angles reproduce the exact energy levels) indicate that CI is here negligible.

These methods are being extended to higher members of the Sn isoelectronic sequence, for which branching fraction measurements do not exist. These results indicate that CI is also small for these systems, and the relative intensities from the same upper level could be used as calibration standards. If lifetime measurements for the individual upper levels were also made, then any transition in the manifold could be used as a calibration standard. The accelerator energy for these in-beam line standards could be tuned to match the velocity of the measured ion so as to match Doppler shifts, and thus an intensity calibration of the detection apparatus in the desired wavelength range could be achieved. A test of this calibration method is currently underway, in which branching fractions for astrophysically significant transitions in singly ionized sulfur in the wavelength region 900-1200 Å are being measured by beam foil methods. To accomplish this, the optical system is first calibrated by accelerating tellurium ions, and using known radiation standards in Sn-like Te^{2+}, for which the relative line strengths have been accurately deduced from spectroscopically determined mixing angles.

Slide 19

Intermediate Coupling Specification of Branching Fractions

Bi II $6s^26p^2 - 6s^26p7s$

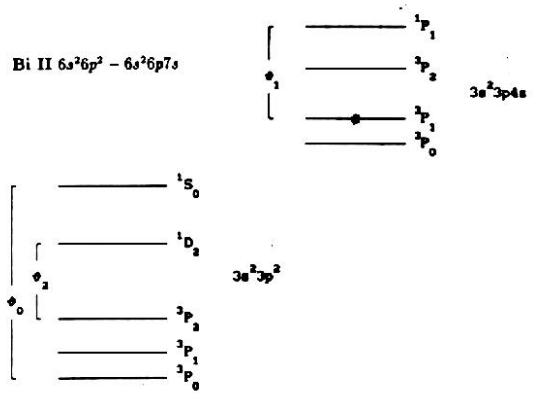

$$< {}^3P_0 \,|r|\, {}^3P_1^o >= -\sqrt{20}\cos(\theta_1 + \theta_0) < p^2|r|sp >$$

$$< {}^3P_1 \,|r|\, {}^3P_1^o >= \sqrt{15}\cos\theta_1 < p^2|r|sp >$$

$$< {}^3P_2 \,|r|\, {}^3P_1^o >= 5(2\sin\theta_1 \sin\theta_2 + \cos\theta_1 \cos\theta_2) < p^2|r|sp >$$

$$< {}^1D_2 \,|r|\, {}^3P_1^o >= -5(2\sin\theta_1 \cos\theta_2 - \cos\theta_1 \sin\theta_2) < p^2|r|sp >$$

$$< {}^1S_0 \,|r|\, {}^3P_1^o >= -\sqrt{20}\sin(\theta_1 + \theta_0) < p^2|r|sp > .$$

Slide 20

Table 7.1. Comparison of semiempirical (S) and measured (M) branching fractions (in %) for ns^2np^2-$ns^2npn's$ transitions in neutral atoms.

Transition	Si I		Ge I		Sn I	
	BF(S)	(M)	BF(S)	(M)	BF(S)	(M)
$^3P_0' \leftarrow {}^3P_1^{o\prime}$	33.3	33.3(3)	31.2	32.5(16)	32.3	27
$^3P_1' \leftarrow$	24.7	24.7(4)	21.2	22.1(11)	17.5	17
$^3P_2' \leftarrow$	41.1	40.7(4)	38.1	37.1(19)	39.7	39
$^1D_2' \leftarrow$	0.88	1.2(1)	8.8	8.1(8)	10.0	17
$^1S_0' \leftarrow$	0.06	<0.20(6)	0.52	0.23(2)	0.5	-
$^3P_1 \leftarrow {}^3P_2^o$	25.2	24.6(3)	26.4	27.2(14)	28.3	22
$^3P_2' \leftarrow$	74.8	74.5(3)	73.1	72.1(14)	68.5	71
$^1D_2' \leftarrow$	0.020	0.027(4)	0.53	0.72(7)	3.2	7
$^3P_0' \leftarrow {}^1P_1^{o\prime}$	0.24	0.30(2)	2.9	4.6(5)	4.2	8
$^3P_1' \leftarrow$	0.25	0.20(2)	3.3	3.6(4)	6.8	4
$^3P_2' \leftarrow$	0.15	0.20(2)	1.0	1.68(17)	0.01	-
$^1D_2' \leftarrow$	92.0	93.4(2)	86.2	86.1(14)	82.2	88
$^1S_0' \leftarrow$	7.4	5.7(12)	6.6	4.0(4)	6.8	-

Coincidence Methods

Coincidence techniques provide a powerful means for measuring lifetimes. However, such methods were difficult to apply to BFS earlier because of the low detection efficiencies in the optical wavelength region, which made accidental coincidences a serious problem. As the acceleration energy (and hence the degree of ionization) is increased, the photon energies become sufficiently large to permit the use of detectors such as those designed for nuclear physics applications.

Slide 21

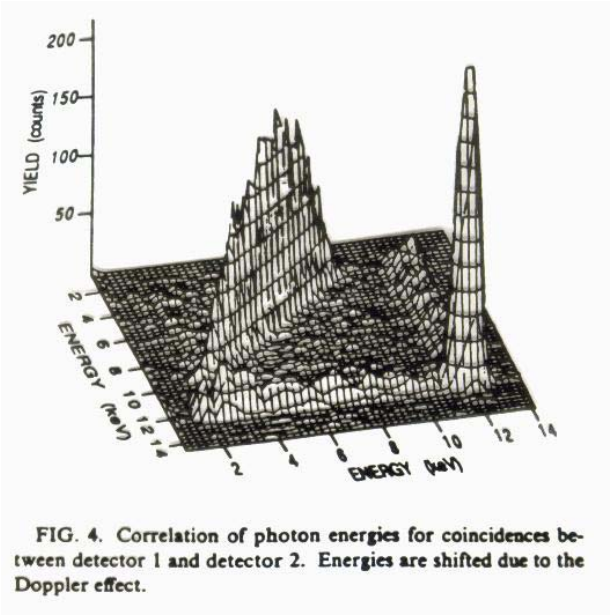

FIG. 4. Correlation of photon energies for coincidences between detector 1 and detector 2. Energies are shifted due to the Doppler effect.

Slide 21 shows an application of coincidence techniques in a beam-foil study of the two-electron bromine ion. Here the ground state is $1s^2\ {}^1S_0$ and the first excited state is $1s2s\ {}^1S_0$. The decay of the upper state by emission of a single electric dipole photon is absolutely forbidden, since both states have zero angular momentum. Thus the level is metastable, and decays either by emission of one magnetic dipole photon, or two electric dipole photons. Through the use of Si(Li) detectors it is possible not only to gate the coincidence between the detection of two photons,

but also to measure the energies of the photons detected. Slide 22 shows a plot of the intensity of the coincidence events plotted as a function of the energies of the individual photons. The diagonal line represents coincidences between the two simultaneously emitted E1 photons, which sum to the total excitation energy of 12 keV. The peak that occurs when both photons have 12 keV represents accidental coincidences between two unrelated M1 photons. The two rows that occur at a single photon energy of 12 keV represent a accidental coincidences between one M1 and one continuum photon. Such applications of coincidence techniques offer many possibilities for new types of measurements of high precision and reliability.

Conclusion

The technique of Beam Foil Spectroscopy has already made significant contributions to the fundamental understanding of atomic structure and its available data base, and it has the potential to provide essential new data of unprecedented accuracy and scope. This work can be carried out with existing accelerator facilities, and the diversity of accelerators available is an important part of the strength of the method.

Recent Reviews

1. L. J. Curtis and I. Martinson, in *Atomic Physics with Heavy Ions,* H. F. Beyer and V. P. Shevelko, editors (Springer-Verlag, Heidelberg, 1999) pp. 197-218.

2. E. Träbert, in *Accelerator-Based Atomic Physics: Techniques and Applications*, S. M.

Shafroth and J. C. Austin, editors (AIP Press, New York, 1998) pp. 567-600.

3. E. H. Pinnington, in *Atomic, Molecular, and Optical Physics Handbook*, G. W. F. Drake, editor (AIP Press, New York, 1996) pp. 213-219.

Discussion

Hyder (Oxford): What differences or improvements would you like to see in accelerators?

Curtis (Toledo): Certainly I want to see continuing development of ion sources. New ways to provide a wide variety of atomic species to give access to any ion Many Accelerator programs are driven, of course, by nuclear physics considerations. The reason we were able to make runs with Uranium was that the nuclear physicists at ATLAS wanted to study Uranium. So actually what I would like to see is for nuclear physicists to have an interest in a lot of different atoms. That would give us the opportunity to study their atomic properties. No one is going to give atomic spectroscopists time on an accelerator for a beam-foil measurement unless nuclear physicists want the same ion. We sometimes come in on Christmas when to pick up on a nuclear physics run, and we are very pleased for that opportunity.

Schneider (Woods Hole): What is the precision with which you can measure lifetimes?

Curtis: It depends on how much you want to spend. We measure to about two per cent on a production scale, and if we really work at it, we can get the level down to better than a tenth of a per cent (in very favourable cases). I'm very glad you asked, because this is a question for nuclear physicists too. We recently wrote a paper on tests of the exponential decay law. As far as I can see the exponential decay law has been tested for short times, it has been tested for long times, it has been tested for a small fraction of a lifetime for a long lived system, and for many many lifetimes of a short lived system. … It has been tested in all kinds of ways, but it's never been tested to better than a per cent. -And yet what we are doing is to assume the law is exact, and the only uncertainties are experimental. Decay curves are measured very carefully and highly precise lifetimes are quoted (I have seen parts in ten to the fifth, parts in ten to the sixth quoted). Yet I have seen no evidence that anyone has ever tested the decay law for small fluctuations on the one tenth of a per cent level in the intermediate region of a few e-folding times. So my question is on the ultimate precision of the exponential decay law. In atomic physics we certainly we have quantum beats superimposed sometimes which clearly give short term oscillations about the exponential law. In what situations can we really separate the excitation Hamiltonian from the decay Hamiltonian? Kristina Stenström talked about this earlier using AMS, which seems like a very good way to test this. With AMS you can both measure the number that are left and the number which are decayed, and if you can put that together it seems that you could get a more inclusive measurement. I don't know how other people feel about this aspect of quantum

mechanics, but when I read about the Weisskopf-Wigner law I get the feeling I'd like to take a shower. I see things like replacing integrals which are bounded below but not above by a- lower infinity. It seems that what they have done is to accept as an experimental fact that the exponential decay law is exactly valid and see what assumptions are needed. It is not a consequence of quantum mechanics, but is forced on it by the belief that there is experimental confirmation. By the uncertainty principle, the lifetime itself provides a limit to the accuracy to which a spectral energy can be measured. Is there no commutation relation that places a limit on the ultimate accuracy to which a lifetime can be measured? It seems like a fundamental quantum mechanical question.